Bistatic scattering in sediments: comparison of model and scaled tank experiments at 238 kHz

R. Howey and P. Blondel

University of Bath, Department of Physics, Claverton Down, BA2 7AY Bath, UK
rph23@bath.ac.uk

Multiple-aspect scattering is increasingly used to investigate seabeds and objects, buried or not. However, high-frequency scattering processes on/in sediments need to be better understood, particularly when the structure and/or composition of these sediments is not fully homogeneous. Scaled tank experiments were conducted with a 238-kHz sonar (10° beamwidth) imaging a silt seabed at 45°. Scattering angles varied between ~16° and ~70° (50 distinct values); bistatic angles varied 40° either side of in-plane with a 2.5° step (33 distinct values). Bottom returns were picked through two methods (automatic and manual) and converted into scattering strengths. This large dataset was compared with the APL-UW model for bistatic scattering, intended for 10-100 kHz but successfully tested at 240 and 455 kHz by other workers. Recursive fitting of model parameters to the experimental values assesses the influence of sediment variations (backed by microscope measurements) and the importance of even small tilts in the surface of the sediments. More importantly, they show the importance of the beam pattern and the sidelobes in the accurate calculation of bistatic scattering strengths. These results can be used to further validate scattering models as well as to design future surveying strategies.

1 Rationale

Recent uses of bistatic sonars show the advantages of decoupling transmitter and receiver(s) to optimise the information from seabed and target scattering. However, high-frequency scattering needs to be better understood, especially in complex, multiple-target environments (e.g. dumpsites or highly cluttered seabeds) where the characteristics of the seabed can greatly influence target scattering. Sea trials are paramount in providing acoustic measurements to validate scattering models and show the different processes involved, but they are expensive, difficult to conduct and fraught with difficulties. Laboratory experiments are complementary, because of the fully controlled environment and the repeatability of the measurements. They can also be used to optimise data collection strategies at sea. The imaging frequencies (> 10 kHz) to be investigated, and the finite dimensions of the tanks (decametre-scale usually), mean that these experiments most often need to be scaled.

The experimental dataset used here extends those presented in earlier studies [1,2], and it is presented in Section 2. Section 3 explains the analysis of the raw scattered waveforms, and the interest of an automatic approach for scattering strengths. Section 4 compares these results to the APL-UW model, and Section 5 discusses the role of sediment mixing and how this compares with similar studies. Finally, Section 6 concludes by showing how these results can be adapted to the processing of field measurements in non-homogeneous terrains.

2 Scaled bistatic experiments

Simple laboratory experiments were first conducted in Bath in 1999-2001 to investigate bistatic scattering in a highly controlled and stable laboratory setting [3,1]. Bistatic scattering from silt were compared with predictions from the APL-UW model [4]. The model's predictions for in-plane scattering agree very closely with the experiments [1]. Away from in-plane scattering, at bistatic deviations of 30°, 60° and 90°, the model seems to overestimate scattering. Experimental results also often showed a small increase in return strength for specular geometries. Most likely causes for model/data discrepancies were assessed as the actual interface roughness (not measured directly, but inferred from the grain size using the relations given with the APL-UW model) and, to a lesser extent, the approximation of scattering areas as constant. These experiments were extended in 2002-2005 using more seabed types, with and without targets, and investigating a much wider range of geometries [2,5].

The setup was designed to be a scaled version of the SITAR sea trials site in Möja Söderfjärd (Sweden), with a scaling factor of approximately 10:1. The underground tank was 5.00 m long, 1.54 m wide and 1.80 m deep. The water depth was kept constant at 1.45 m. The sediment tray used in this study was filled with thoroughly degassed silt, 14 cm deep. For a scaling factor of 10:1, this matches the soft muddy sediments found in Möja Söderfjärd [6]. Careful preparation ensured all sediments were water-saturated and their surfaces were as smooth as possible [7]. The imaging transducer was transmitting at 238 kHz and tilted at a fixed incidence angle of 45°, 0.5 m from the target. The scattered signal was measured with an omnidirectional hydrophone mounted on a robotic system (Figure 1). To complement previous measurements [3,5], the range of scattering and bistatic angles was significantly extended. Scattering angles varied between ~16° and ~70° (50 distinct values); bistatic angles varied 40° either side of in-plane with a 2.5° step (33 distinct values).

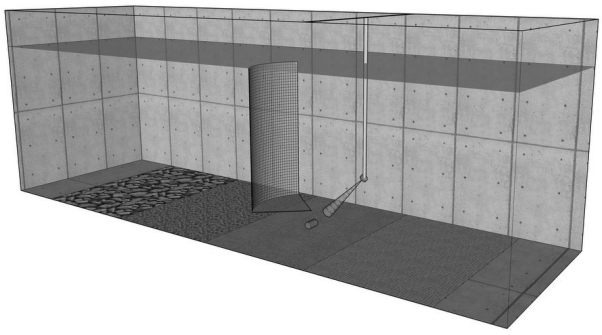

Fig.1 General view of the experimental tank. The imaging transducer is fixed, imaging the silt bed at 45°. The receiver describes a grid covering 1650 different combinations of scattering and bistatic angles.

3 Analyses

3.1 Waveform processing

The output signal was amplified, band-pass filtered and averaged over 100 waveforms for each geometry. The waveforms were all measured over the same duration and normalised to the amplitude of the direct arrival, to account for slight differences in source level and/or propagation paths. They were then zero-banded to remove the direct signal and their envelopes were calculated using the Hilbert transform. The scattering strengths of each target are deduced using the standard sonar equation [8]:

$$SS = RL - SL + TL_1 + TL_2 - 10\log A \qquad (1)$$

where SS is the average scattering strength (dB re 1 m_2) over the ensonified area; RL is the reverberation level (dB re 1 µPa) on the hydrophone, SL is the source level (178 dB re 1 µPa at 1 m in this case), TL_1 is the transmission loss (in dB re 1 m) from the source to the bottom, TL_2 is the transmission loss (in dB re 1 m) from the bottom to the hydrophone, and A is the ensonified area (in m^2) associated with the 3-dB beam pattern and pulse length.

Because of the geometry used, TL_1 is constant and TL_2 will vary slightly with hydrophone position. A will be the largest contributor to uncertainties in Eq.(1). The instantaneous ensonified area covers 0.0172 m^2 but this needs to be modulated by the pulse length (39.2 µs) and beamwidth, and the exact scattering area will be the intersection of two ellipsoids with source and receiver as foci [9]. The sidelobes will add to this area, and this will be particularly noticeable at high bistatic deviations (see Section 4 for details).

3.2 Automatic picking of bottom returns

The reverberation level is calculated from the average signal strength, using the 70-dB pre-amplification before recording and the hydrophone sensitivity (-211 dB re 1 V/µPa). For this, the signal scattered from the seabed needs to be identified and separated from spurious reflections, e.g. from the sidewalls or the water surface. The number of geometries investigated is high (1650) and as analyses of silt returns will be followed by analyses from target returns in many more configurations; there is clearly a need for automating the picking of bottom returns.

The signals' envelopes were smoothed with a 13-point moving average to filter out the higher-frequency components. Inflection points are identified in the time-domain signal, creating a highly simplified version of the original envelope by only keeping its "peaks" and "valleys". The process is applied recursively, checking that there always is a "valley" between the direct arrival (shortest geometric path) and the expected seabed peak (second shortest geometric path). To correctly identify the signal scattered from the seabed, the "peaks" identified in the final reduced signal set are ranked according to several expected criteria (e.g. amplitude relative to other "peaks" and background noise, width, matching expected return times from the local geometry, etc.). One-to-one comparison with manual picking of seabed returns shows a very good accuracy (Figure 2) and this method will be of particular use when processing the next series of experiments. In combination with the other parameters outlined in Eq.(1), these returns are used to calculate the bistatic scattering strength of the seabed.

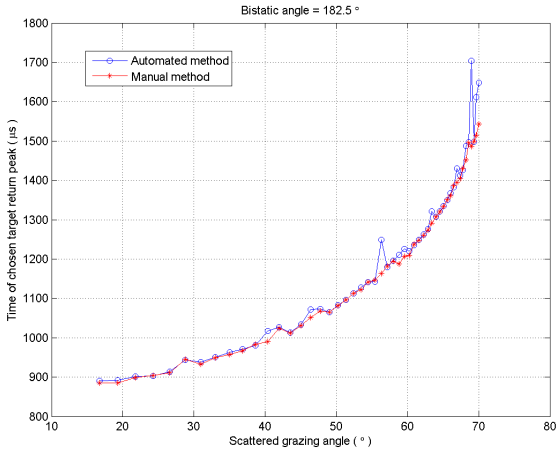

Fig.2 Comparison of manual and automatic picking of the seabed/target return.

4 Model/data comparisons

These measurements of bistatic scattering were compared to the APL-UW model. This model was selected because it had already shown a reasonable agreement with data acquired in sea trials (e.g. [10,11]). Although originally intended for frequencies between 10 kHz and 100 kHz, it has been shown in some cases to work for higher frequencies, e.g. 240 kHz [12] and 455 kHz [13]. It is also easier to implement than other models, not requiring very detailed information about seabed geotechnical parameters. This model has been detailed in many reports and articles (e.g. [4]). Bistatic scattering is attributed to both the roughness of the seabed and volume inhomogeneities within the sediment. The scattered intensity is therefore a sum of two terms: one term is proportional to the roughness-scattering cross section (a smooth interpolation between the Kirchhoff cross section near the specular direction and the perturbation-theory cross-section elsewhere), and the other term is proportional to the volume-scattering cross-section.

The interface between the water and the sediment is assumed to be an isotropic, 2-D Gaussian random process completely determined by a spectral density that follows a simple power law in wave number (with exponent γ_2 and overall spectral level w_2). Acoustic penetration of the seabed is assumed slight, so that sediment volume scattering can be described as a surface process and quantified by an effective interface scattering cross-section. A major assumption is that the sediment can be treated as a lossy fluid: any effects due to elasticity or porosity are neglected. It is further assumed that there are no gradients in sediment properties, apart from the random fluctuations responsible for volume scattering. Thus, the sediment can be characterised by three parameters: mass density ρ, sound

speed (or the ratio v to the sound speed in water), and the acoustic absorption coefficient α_b.

The spectrum of volume inhomogeneities is also assumed to follow a power-law form, which adds three parameters to the model: the exponent of the power law γ_3, a parameter w_3 that sets the overall spectral level, and a parameter μ expressing the ratio of compressibility to density fluctuations. Volume scattering is assumed to be weak in the sense that the scattered field is much smaller in magnitude than the incident field.

The APL-UW model has been used to predict the bistatic scattering strengths expected from this silt seabed, deriving all parameters from the mean grain size of the seabed. The results (Fig. 3) show smooth variations with scattering angle and with bistatic angle. The highest returns occur around the specular angle (45°), in the line of sight between the transmitter's main axis, the seabed and the receiver.

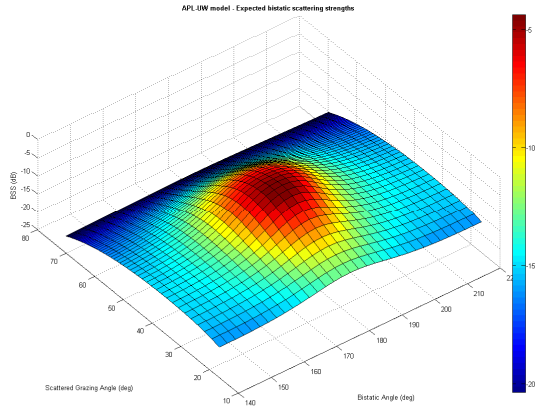

Fig.3. Scattering strengths predicted by the APL-UW model for a flat silt seabed and for this particular range of scattering and bistatic angles. The incident angle is 45°.

Using the experimental results, bistatic scattering strengths were derived using Eq. (1). Bistatic scattering is still stronger in the main direction, at near-specular angles, and it decreases with bistatic angles away from the line of sight. However, a direct comparison with the APL-UW model shows a constant offset and, more importantly, some clear discrepancies (Fig. 4).

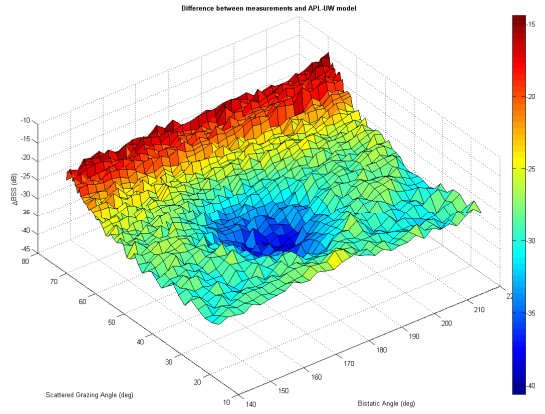

Fig.4. Difference between the experimental measurements of bistatic scattering strengths and the expectations from the APL-UW model.

The discrepancies between our measurements and the APL-UW model occur mostly around the specular angle, over a range of angles commensurate with the beamwidth of the imaging transducer (~10°). This would suggest an influence from the beam pattern of the imaging transducer. Other factors coming into play would be the actual tilt of the surface (deviation from the flat seabed assumption), and the average grain size (does one grain size describe all sediments in the scattering area?).

5 Discussion

The tank experiments were conducted in a finite environment. Spurious reflections from the sides of the tank and from the water surface can, in some cases, occur at the same time as the main return from the silt seabed and affecting its level. These measurements can be filtered out, but only account for a small fraction of the 1650 measurements presented here.

The larger differences between actual and expected bistatic scattering strengths occur slightly off the specular angle (i.e. scattering angle of 45° and bistatic angle of 180°, i.e. in plane). This can be explained by a slight local tilt of the silt surface; this tilt would be of ~5° in the direction perpendicular to the imaging direction. This is likely, especially as a similar effect is presented in [12] where coarsely raked seabeds severely changed the scattering strengths at particular angles. But this still does not account for the scale of these differences.

This localised strong difference (Fig. 4) suggests that the beam pattern plays a role. In the tank experiments, the transducer used had a circular main beam with a 3-dB beamwidth of 10°. The main beam intersected the sediment in the shape of an ellipse with an area of 0.0171 m^2, though due to the short pulse length of 39.2 µs, a maximum of 0.0096 m^2 was ensonified at one time. In addition to the main beam, side lobes were present. They are symmetrical at 12° from the main beam's centre, with 3-dB beamwidths of 5° and 6° respectively, and levels 14.5 dB and 16 dB lower than the main beam [1]. The intersection of the side lobes and the sediment correspond to ellipses with areas of 0.0041 m^2 and 0.0060 m^2 respectively. The order of magnitude suggests their contribution can be significant at a range of bistatic and scattering angles.

The exact calculation of the bistatic scattering area A is not straightforward. [14] gives an approximation in the backscatter case and [15] mentions the effect of the scattering area, particularly with contributions from side lobes, when dealing with short pulse lengths. Eq. (1) shows the direct role of A and how its inaccuracy can affect the final results. We implemented in Matlab the analytical derivations of the scattering area in a bistatic configuration done by [9], with a grid interval of 1 mm^2. These results are presented in Fig. 5. The contribution from the main beam is constant in most configurations (Fig. 6). The difference between the actual scattering area and that assumed previously can be as high as 58% (for specular, in-plane scattering) and varies significantly throughout all experimental configurations. Accounting for sidelobes and pulse length shows that the main beam contributes between ca. 50% and 100% of the overall scattering areas, further

confirming the importance of the sidelobes in calculating the scattering strengths, and in interpreting the results from bistatic experiments.

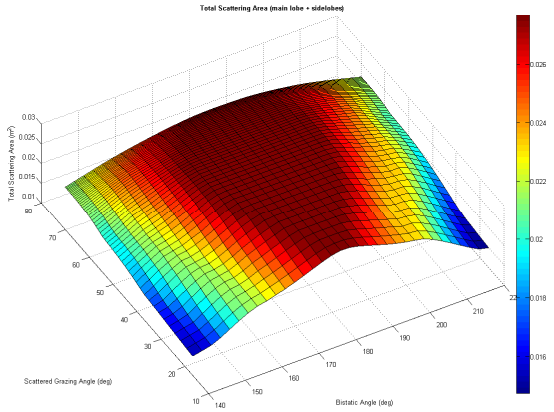

Fig.5. Instantaneous scattering areas for both main beam and sidelobes.

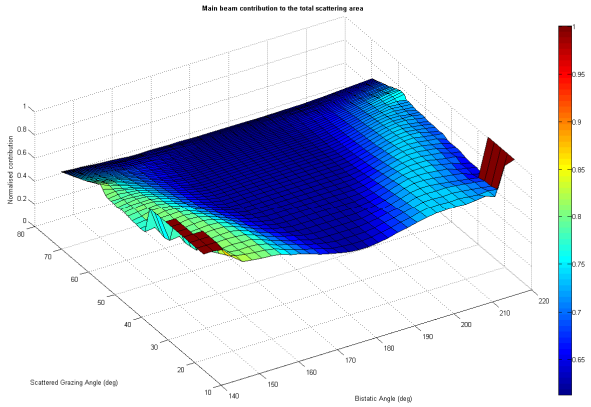

Fig.6. Normalised contribution of the main beam to the entire scattering area.

Another important factor to consider is the assumption that the silt seabed was homogeneous. Localised samples were taken over areas of a few square centimetres. The silt sediment appeared stratified, and made up of two grain sizes (Fig. 7, inset). The nominal grain diameter was 0.05 m, but high-magnification microscope measurements yielded actual values of 0.062 ± 0.005 mm (with 95% confidence). Similar measurements in the neighbouring sand tray showed the nominal grain diameter of 1-2 mm was in fact averaging 0.941 ± 0.030 mm. There seems to be some slight contamination of silt and sand sediments, at least in the sample taken. This might have some direct effect on the expected scattering strengths, both for the input parameters and for the expected micro-scale roughness. To account for potential sediment mixing, ensemble-average simulations used the APL-UW model with these variations around the mean grain diameter (Fig. 7). Variations were however not large enough to further explain the discrepancy shown in Fig. 4. The tilt in the seabed only accounts for local deviations, and variations in the scattering area (and the influence of the main beam) seem therefore to account for most of the observed variations.

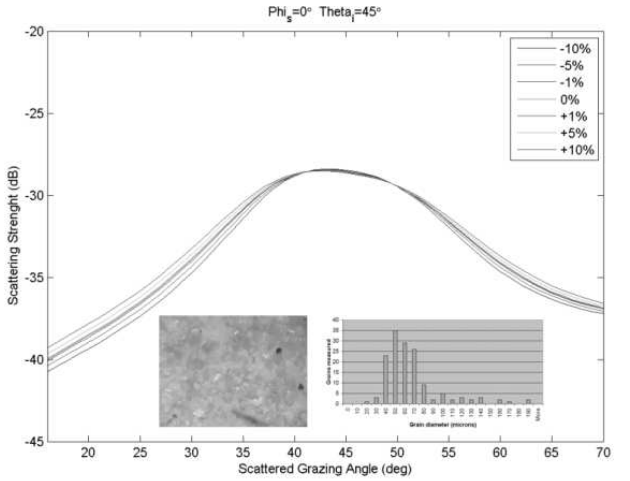

Fig.7 Ensemble-average simulations were run to account for the sediment mixing suspected. Inset: (left) close-up view of the silt sample; (right) histogram of grain sizes in the sample area. These simulations do not explain the differences observed around the specular angle.

6 Conclusion

The investigation presented here is based on earlier scaled tank experiments, in which a silt seabed was imaged by a narrow-beam sonar at 238 kHz. The scattered sound was measured by a hydrophone describing 1650 different configurations. Scattering angles varied between ~16° and ~70°; bistatic angles varied 40° either side of in-plane with a 2.5° step. Bottom returns were picked through two methods (automatic and manual), in preparation for the analyses of other datasets concerned with target scattering. The automatic picking method gave excellent results when compared with manual picking of the seabed returns.

These returns were then converted into scattering strengths. The large dataset generated was compared with the APL-UW model for bistatic scattering, intended for 10-100 kHz but successfully tested at 240 and 455 kHz by other workers [12,13]. Although the experimental measurements are consistent, they show systematic differences with the model, namely a near-constant offset and larger deviations near the specular angle. A small, local tilt of the seabed can explain the angular deviation, and a small amount of sediment mixing can explain small deviations from expected values. Most of the deviations seem to come from the actual scattering area, a compound of the main beam and the two sidelobes. This complements earlier observations, e.g. by [16] in sea trials and [1] in other tank experiments. These results strongly hint that the largest sources of disagreement between measurements and models of high-frequency bistatic scattering are inaccuracies in calculating instantaneous scattering areas and variations in seabed roughness. These results can be used to further validate scattering models. By considering the characteristics of the imaging sonar as well as unexpected seabed variations, they can also be used to design future surveying strategies.

Acknowledgments

The scaled laboratory experiments were conducted by PB with N. Jayasundere and M. Cosci (U. Bath) as part of the European Union project SITAR (contract #EVK-3-CT2001-00047). Prof. N.G. Pace (U. Bath) assisted in the calculation of the instantaneous scattering areas and offered helpful suggestions to relate these observations of bistatic scattering to other studies in similar conditions.

References

[1] Ph. Blondel, P. McCloghrie, N.G. Pace, G.J. Heald and R. Brothers, High-frequency bistatic bottom scattering: Modelling & experimental studies, Proc. 6th ECUA, 21-29. Gdansk (2002)

[2] Ph. Blondel, P.F. Dobbins, N. Jayasundere, M. Cosci, 'High-frequency bistatic scattering experiments using proud and buried targets', *in* "Experimental Acoustic Inversion Techniques in Shallow-Water", A. Caiti, R. Chapman, S. Jesus, J.-P. Hermand (eds.), Springer, 155-170 (2006)

[3] Ph. Blondel, N.G. Pace, G.J. Heald, R. Brothers, High-frequency bistatic scattering: comparison of tank and sea experiments, Proc. IOA, Vol. 23(2), 276-282. SOC (2001).

[4] APL-UW High-Frequency Ocean Environmental Acoustic Models Handbook. TR 9407 (Oct. 1994)

[5] Ph. Blondel, D. Fang, A. Smith and N. Jayasundere; 'High-frequency bistatic imaging of proud targets – Influence of target orientation and type'; Proc. 2nd UAM. Heraklion (2007).

[6] Ph. Blondel and A. Caiti (eds.); 'Buried Waste in the Seabed – Acoustic Imaging and Bio-toxicity (Results from the European SITAR project)', Springer-Praxis (2007).

[7] Ph. Blondel and N.G. Pace, Scaled tank experiments: Seabed and target scattering at high frequencies, Proc. 1st UAM. Heraklion (2005).

[8] Urick, R. J., 1983. *Principles of Underwater Sound.* 3rd Edition. USA: McGraw-Hill, Inc

[9] Pace. N.G., personal communication. April 21, 2008

[10] K.L. Williams, D.R. Jackson: Bistatic bottom scattering: Experimental results and model comparison for a carbonate sediment, in N.G. Pace, E. Pouliquen, O. Bergem, A.P. Lyons: High-Frequency Acoustics in Shallow Water, Lerici, NATO, 1997

[11] K.L. Williams, D.R. Jackson: Bistatic bottom scattering: Model, experiments and model/data comparison, J. Acoust. Soc. Am. 103, pp. 169-181, 1998

[12] Choi, J.W., J. Na, W. Seong, "240-kHz Bistatic Bottom Scattering Measurements in Shallow Water" IEEE J. Ocean. Eng., 26(1), pp.54-62, 2001

[13] ANSTEE, S., Removal of range-dependent artifacts from sidescan sonar imagery. Technical Report DSTO-TN-0354, 2001

[14] McKinney, C.M., C.D. Anderson; "Measurements of backscattering of sound from the ocean bottom. J. Acoust. Soc. Am., 36(1), pp.158-163, 1964

[15] Canepa, G., E. Pouliquen, L. Pautet, N.G. Pace; "Bistatic scattering from the seabed at high frequency", Proc. ECUA-2004, p. 595-600, 2004

[16] Canepa, G., N.G. Pace, E. Pouliquen; "Field measurements of bistatic scattering strength of a sandy seabed at 118 kHz", Proc. ECUA-2002, p. 183-188, Gdansk, Poland, 2002